



Approximate 1 hour per response, including the time for reviewing instructions, searching existing data sources, gathering and reviewing the data, and completing and reviewing the collection of information. Send comments regarding this burden estimate or any other aspect of this collection of information, including suggestions for reducing this burden, to Washington Headquarters Office, Paperwork Project, 1215 Jefferson Davis Highway, Suite 1204, Arlington, VA 22202-4302, and to the Office of Management and Budget, Paperwork Project, 1215 Jefferson Davis Highway, Suite 1204, Arlington, VA 22202-4302, and to the Office of Management and Budget, Paperwork Project, 1215 Jefferson Davis Highway, Suite 1204, Arlington, VA 22202-4302, and to the Office of Management and Budget, Paperwork Project, 1215 Jefferson Davis Highway, Suite 1204, Arlington, VA 22202-4302.

2

1. Report Type and Dates Covered. Final - Proceedings	
4. Title and Subtitle. Shear Effects on Ocean Acoustic Propagation Due to Step-Periodic Roughness Along the Ocean Bottom Interface	5. Funding Numbers. Contract Program Element No 0601153N Project No 03202 Task No 360 Accession No DN257033 Work Unit No 12211D
6. Author(s). Stanley A. Chin-Bing and Joseph E. Murphy*	8. Performing Organization Report Number. PR 91:114 221
7. Performing Organization Name(s) and Address(es). Naval Research Laboratory Center for Environmental Acoustics Stennis Space Center, MS 39529-5004	10. Sponsoring/Monitoring Agency Report Number. PR 91:114 221
9. Sponsoring/Monitoring Agency Name(s) and Address(es). Naval Research Laboratory Exploratory Development Program Group Stennis Space Center, MS 39529-5004	
11. Supplementary Notes. Published in IMACS, Computational Acoustics.	
12a. Distribution/Availability Statement. Approved for public release; distribution is unlimited.	12b. Distribution Code.
13. Abstract (Maximum 200 words). Low-frequency ocean acoustic propagation can be affected by backscatter from rough ocean bottoms and by compressional-shear wave conversions within the ocean bottom. Numerical simulations have been performed that include the effects of such backscattering and loss mechanisms. A full-wave range-dependent finite-element ocean seismo-acoustic computer model (SAFE) was used together with a simulated rough ocean bottom structure that supported compressional and shear wave speeds as well as compressional and shear wave attenuations. Step-periodic changes in depth and range along the water-bottom interface were used to simulate ocean-bottom roughness. A numerical example was used to illustrate the combined effects of ocean-bottom shear and roughness, and to give insight into these complicated processes.	
<p>08 4 11 029</p> <p>93-07691</p> <p>SPR</p>	
14. Subject Terms. Acoustic waves, elastic waves, seismic waves	15. Number of Pages. 6
	16. Price Code.
17. Security Classification of Report. Unclassified	18. Security Classification of This Page. Unclassified
19. Security Classification of Abstract. Unclassified	20. Limitation of Abstract. SAR

DTIC
SELECTED
APR 14 1993
S D

ISSN 1067-0683
Volume 2, 1993
Section B

Mathematical Modelling and Scientific Computing

Affiliated with the International Association for Mathematical and Computer Modelling

EDITOR-IN-CHIEF

Xavier J. R. Avula

Mathematical Modelling
and
Scientific Computing
Volume 2, 1993
Science and Technology

THE EIGHTH INTERNATIONAL CONFERENCE

College Park, Maryland, U. S. A. April 1991



PRINCIPIA SCIENTIA
St. Louis . Madison

**BEST
AVAILABLE COPY**

ACOUSTICS

SHEAR EFFECTS ON OCEAN ACOUSTIC PROPAGATION DUE TO STEP-PERIODIC ROUGHNESS ALONG THE OCEAN BOTTOM INTERFACE

Stanley A. Chin-Bing[†] and Joseph E. Murphy[§]

[†] Numerical Modeling Division, Naval Oceanographic and Atmospheric Research Laboratory, Stennis Space Center, MS 39529-5004, U.S.A.

[§] Department of Physics, University of New Orleans, New Orleans, LA 70148, U.S.A.

ABSTRACT

Low-frequency ocean acoustic propagation can be affected by backscatter from rough ocean bottoms and by compressional-shear wave conversions within the ocean bottom. Numerical simulations have been performed that include the effects of such backscattering and loss mechanisms. A full-wave range-dependent finite-element ocean seismo-acoustic computer model (SAFE) was used together with a simulated rough ocean bottom structure that supported compressional and shear wave speeds as well as compressional and shear wave attenuations. Step-periodic changes in depth and range along the water-bottom interface were used to simulate ocean-bottom roughness. A numerical example was used to illustrate the combined effects of ocean-bottom shear and roughness, and to give insight into these complicated processes.

KEYWORDS

Shear waves; seismo-acoustics; ocean acoustics; wave propagation; backscatter.

INTRODUCTION

Recently, the finite element (FE) method has been applied (Murphy and Chin-Bing, 1988, 1989, 1991; Chin-Bing and Murphy, 1988, 1990) to develop several computer models that calculate the complex pressure field resulting from acoustic and elastic propagation and scattering in a inhomogeneous ocean with range-varying boundaries (sea surface and ocean bottom). Although these computer models are computational intensive, they have been verified to give benchmark accurate predictions of the underwater complex pressure field. In this paper we first briefly review the salient points leading to the developments of these FE acoustic and elastic ocean propagation models. Next, further developments and implementations regarding our seismo-acoustic FE model, SAFE (Murphy and Chin-Bing, 1991), are presented. The SAFE model includes the ocean bottom as an anelastic medium, having range and depth dependence in compressional and shear speeds and in compressional and shear attenuations. Finally, we apply the SAFE model to simulate a typical shallow water scenario with a rough ocean-bottom interface overlying a shear supporting media. Further verification of the accuracy of the SAFE model is also presented.

In the development of the scalar FE ocean acoustic model, FOAM (Murphy and Chin-Bing, 1988, 1989), the starting point is the inhomogeneous Helmholtz equation,

$$\rho \nabla \cdot (\rho^{-1} \nabla P) + k^2 P = -\delta(\mathbf{r} - \mathbf{r}_S) \quad (1)$$

The solution to this equation (with appropriate boundary conditions) gives the time-harmonic complex pressure field from a unit-strength point-source of angular frequency ω at position \mathbf{r}_S in an inhomogeneous ocean. A three-dimensional ocean environment, axially symmetric about a vertical line passing through the source, is assumed. In Eq. (1), written in cylindrical coordinates, $\rho = \rho(z, r)$ is the density, $k = k(z, r) = \omega/c(z, r)$ is the wavenumber, and $c(z, r)$ is the sound speed. Attenuation is included as an imaginary term in the complex wavenumber.

FOAM simulates a typical ocean acoustic scenario as follows: The acoustic source is arbitrarily placed in the water column or fluid ocean bottom; the sound speeds, in the water and in the fluid

ocean bottom, may vary with both depth and range; the depth of the water-bottom interface may vary with range; the acoustic pressure vanishes at the air-water interface (pressure release surface); beyond some maximum depth the ocean bottom is assumed to be homogeneous; beyond some maximum range the sound speed profiles are assumed not to vary; then, along the right and bottom computational boundaries, FOAM imposes an approximate boundary condition (radiation condition) to prevent energy reflecting from the computational boundaries back into the interior.

In using the FE method to solving the ocean acoustic (fluid) wave equation, the differential equation and its unknown solution are replaced by a system of algebraic equations in terms of parameters that define an approximate solution. The domain is partitioned into non-overlapping *elements* and assumes a simple form for the approximate solution within each element. These local representations are then joined together by using the appropriate physical continuity conditions to provide a global solution. The ocean acoustic wave equation and the associated boundary conditions give a system of matrix equations which are sparse, banded, and symmetric.

FOAM uses a FE grid composed of triangular elements and computes the complex pressure values at the each node of the grid. The FE grid is formed so that the boundaries of the appropriate interior elements coincide with the actual physical interfaces, thus giving a more physically correct computational model. Discontinuities in density, sound speeds, etc. that normally occur in going across the water-bottom interface are thus easily included in FOAM.

THE SEISMO-ACOUSTIC FINITE-ELEMENT MODEL: SAFE

The FE methods employed in creating the underwater acoustic (compressional) model, FOAM, have been used to create the Seismo-Acoustic Finite Element model, SAFE, that includes the coupled effects of shear waves and compressional waves, together with shear and compressional attenuations. The SAFE model departs from FOAM in three major ways: (1) Rectangular elements are used (Fig. 1) rather than the triangular elements used in FOAM; (2) Displacements are calculated by the SAFE model and the complex pressure field obtained from derivatives of these displacements – FOAM solves for the complex pressures directly; and, (3) SAFE has an inhomogeneous anelastic ocean bottom – FOAM assumes an inhomogeneous fluid ocean bottom.

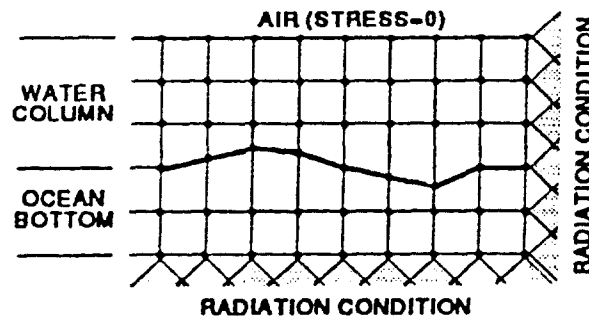


Fig. 1. SAFE finite element grid with boundary conditions. Element nodes are adjusted to lie along the water-bottom interface.

2-D Elastic Equations of Motion

The equations for a 2-D elastic medium (in the xy -plane) can be written in matrix form as,

$$\mathbf{f} = -\omega^2 \rho \mathbf{d} - \mathbf{D}^T \mathbf{C} \mathbf{D} \mathbf{d} \quad (2)$$

$$\mathbf{t} = \mathbf{N}^T \mathbf{C} \mathbf{D} \mathbf{d} \quad (3)$$

where: $\mathbf{d} = [u, v]^T$ is a column matrix containing node displacements u , and v ; $\mathbf{f} = [f_x, f_y]^T$ is a column matrix containing horizontal and vertical body forces, f_x , f_y , respectively; \mathbf{C} is a square matrix containing the elasticity constants, and $\mathbf{t} = [t_x, t_y]^T$ is a column matrix composed of the boundary (traction) forces. \mathbf{D} is a matrix of differential operators (partial derivatives with respect to the x and y coordinates) and \mathbf{N} is a matrix composed of x and y components of the unit normal vector, $\mathbf{n} = (n_x, n_y)$, to the boundary. They are defined by:

$$\mathbf{N} = \begin{bmatrix} n_x & 0 & n_y \\ 0 & n_x & n_x \end{bmatrix}^T, \quad \mathbf{D} = \begin{bmatrix} \partial/\partial x & 0 & \partial/\partial y \\ 0 & \partial/\partial y & \partial/\partial x \end{bmatrix}^T \quad (4)$$

For plane strain, $C_{11} = C_{22} = E(1-\nu)/[(1+\nu)(1-2\nu)]$, $C_{12} = E\nu/[(1+\nu)(1-2\nu)]$, and $C_{33} = E\nu/2(1+\nu)$. E is the modulus of elasticity, and ν is Poisson's ratio.

The equations of motion for plane elasticity (equilibrium of stresses, strain-displacement relations, and stress-strain or constitutive relations) are represented by Eq. (2) and the boundary conditions (i.e., traction forces on the boundaries) are represented by Eq. (3). In the SAFE model, axial symmetry is assumed and Eqs. (2) - (4) are written appropriately in cylindrical coordinates.

The bilinear interpolations functions for the rectangular element are $\Psi_1(\xi, \eta) = (1-\xi/a)(1-\eta/b)$, $\Psi_2(\xi, \eta) = (\xi/a)(1-\eta/b)$, $\Psi_3(\xi, \eta) = (\xi/a)(\eta/b)$, and $\Psi_4(\xi, \eta) = (1-\xi/a)(\eta/b)$, where ξ and η are local coordinates, $\xi = x - x_1$, $\eta = y - y_1$, and Ψ obeys the orthogonality conditions and is normalized, i.e., $\Psi_i(\xi_i, \eta_j) = \delta_{ij}$ and $\sum \Psi_i(\xi, \eta) = 1$, where the summation extends from 1 to 4. Using the finite element interpolation for u and v in each individual element, (i.e., $u = \sum u_i \Psi_i$, $v = \sum v_i \Psi_i$, with the summation extending from 1 to 4) yields matrix equations of the form,

$$(\mathbf{K} - \mathbf{M}) \mathbf{U} = \mathbf{F}, \quad (5)$$

$$\text{with, } \mathbf{K} = \int_{\Omega} \mathbf{B}^T \mathbf{C} \mathbf{B} dx dy, \quad \mathbf{F} = \int_{\Omega} \Psi^T f dx dy + \int_{\Gamma} \Psi^T t dS, \quad \mathbf{U} = [u_1, v_1, u_2, v_2, u_3, v_3, u_4, v_4]^T \quad (6)$$

$$\text{and, } \mathbf{B} = \mathbf{D} \Psi, \quad \mathbf{M} = \omega^2 \rho \Psi^T \Psi, \quad \Psi = \begin{bmatrix} \Psi_1 & 0 & \Psi_2 & 0 & \Psi_3 & 0 & \Psi_4 & 0 \\ 0 & \Psi_1 & 0 & \Psi_2 & 0 & \Psi_3 & 0 & \Psi_4 \end{bmatrix}. \quad (7)$$

Different material properties are allowed within each rectangular element. The material constants, C_{ij} , and the density are kept constant within an element, thus allowing all of the integrations required for the \mathbf{K} -matrices to be done analytically. One could include the ability to deform the rectangular elements so that the nodes could follow the range-dependent ocean bottom bathymetry, or any other surfaces across which there are sharp discontinuities in properties. However, numerical integrations would then have to be made for the contributions that these quadrilateral elements would make to the FE system of equations.

The Boundary Integral and Radiating Boundary Conditions

The FE rectangular elements are influenced by neighboring elements and boundaries depending upon whether the elements are interior elements or elements with one or two of its sides on a boundary. Elements within the interior of the FE grid are of the form, $\int \Psi_i t_x dS$ and $\int \Psi_i t_y dS$. These integrals are exactly cancelled by similar terms from a neighboring element. This is due to the condition that the stresses must be continuous. Elements with one or possibly two of their sides on the actual boundary of the computer model are allowed two different boundary conditions: (a) Stress-Free: $t_x = t_y = 0$. This is treated exactly and the boundary term is zero. (b) Radiation Boundary Condition: Waves should propagate through the model's terminating boundaries without reflection. This boundary condition is treated approximately.

In the scalar CW pressure wave model, FOAM, the normal derivative, $\partial P/\partial n$, appears in boundary integrals computed along the bottom and the right side of the computational grid. The approximate radiation condition first used was $\partial P/\partial n = ikP = i(\omega/c)P$, which gives a small effective reflection from the boundary. In the seismo-acoustic model, SAFE, approximate boundary conditions discussed by Kalinowski (DiNapoli, and Deavenport, 1979) are incorporated: $\sigma_n = \rho c_p v_n$ (for normal traction), and $\sigma_t = \rho c_s v_t$ (for tangential traction), where σ_n , σ_t are the normal and tangential stress, respectively; c_p , c_s are the compressional and the shear wave speeds, respectively; and, v_n , v_t are the normal and the tangential components of particle velocity on the boundary, respectively. These conditions for both the scalar wave model and the seismo-acoustic model are exact for plane waves propagating normal to the boundary, i.e., they give "zero" reflection. Numerical reflections from the boundaries do occur for oblique propagating waves; they are eliminated by combining the radiating boundary condition with increased attenuation.

Attenuation

FOAM treats attenuation for CW propagation by using a complex wavenumber, $k = (\omega/c)(1 + i\eta\beta)$, where $\beta = \text{attenuation in dB/wavelength}$, and η is a numerical constant given by $\eta = (40\pi \log_{10} e)^{-1}$.

This is equivalent to defining an effective complex wave speed via $1/c \rightarrow 1/c_{eff} = (1/c)(1 + i\eta)$. In the SAFE model, attenuation is implemented for both compressional waves and shear waves in a similar fashion: $1/c_p \rightarrow 1/c_{p,eff} = (1/c_p)(1 + i\eta\beta_p)$, $1/c_s \rightarrow 1/c_{s,eff} = (1/c_s)(1 + i\eta\beta_s)$

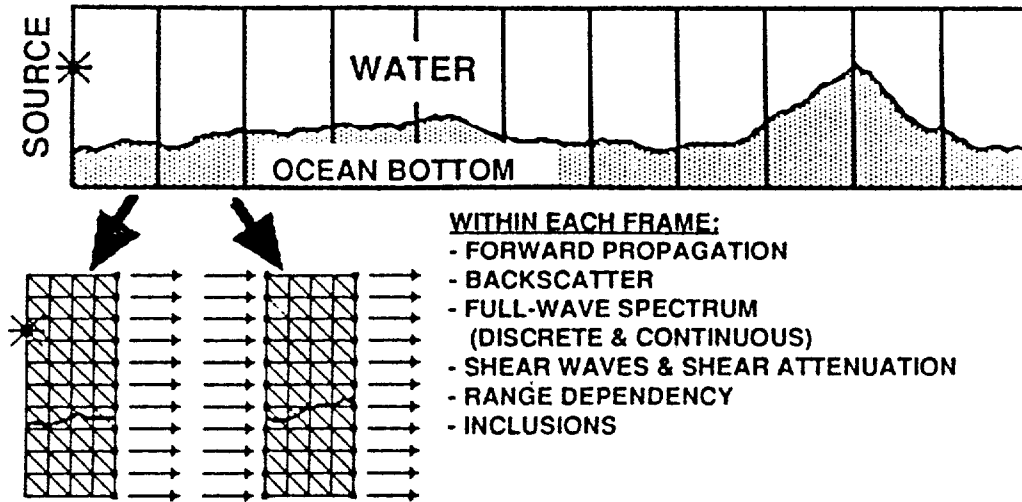


Fig. 2. Marching-frames approach showing how SAFE is solved within each frame and the vertical field from that frame used as the starting field for the next successive frame.

Marching Frames Approach to Long Range Propagation

Figure 2 illustrates how a FE model can be used to predict long-range ocean acoustic propagation. The FE Full-wave Range-dependent Acoustic Marching Elements model, FFRAME, (Chin-Bing and Murphy, 1990) was the first of our FE models to employ this technique. A large "frame" enclosing a region of ocean and ocean bottom is solved by the FE model. The vertical column of pressures from this frame is then used as a starting field for the next large FE frame. By successive application of this technique, the 1-way (outgoing) propagating field can be "marched" to very long ranges while still including the 2-way effects of backscatter losses within each frame. Each frame can be made a different size to accommodate any special ocean features.

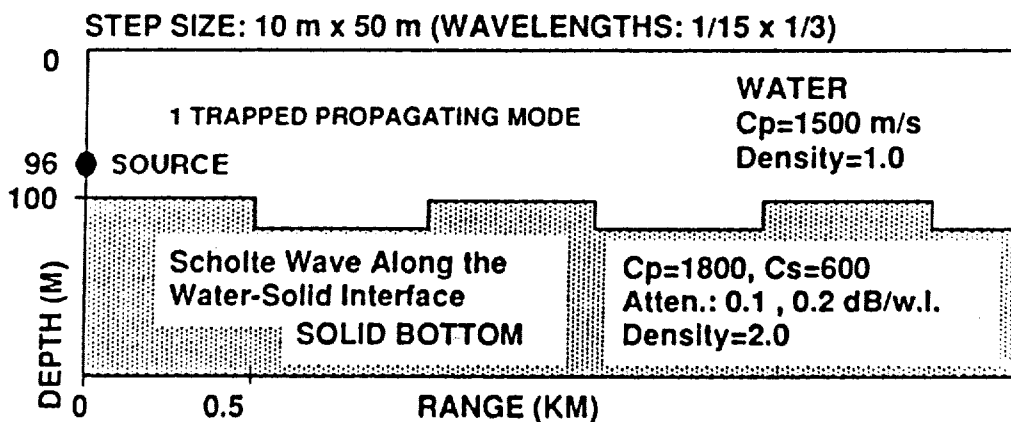


Fig. 3. Step-periodic rough bottom with shear used in the example.

NUMERICAL EXAMPLE

An example given by Schmidt and Jensen (1985) was chosen for a comparison of the SAFE model against a known numerical solution. A 100 m deep homogeneous water column (1500 m/s) overlies a solid homogeneous bottom (compression speed = 1800 m/s, shear speed = 600 m/s, compressional attenuation = 0.1 dB/λ, shear attenuation = 0.2 dB/λ, and a density ratio between bottom and water of 2.0). A 10 Hz acoustic point source is placed at a depth of 96 m

(4 m above the bottom) so as to excite the Scholte interface wave that travels along the water-solid interface. There is one trapped mode in the water column. An interference pattern between the interface (Scholte) wave and the one trapped mode should be evident in the water near the water-solid boundary. Roughness was simulated as shown in Fig. 3 using a step-periodic approach (Evans and Gilbert, 1985). Since the SAFE model can simulate range-dependent shear, the combined effect of roughness and shear on water-borne acoustic propagation can be observed.

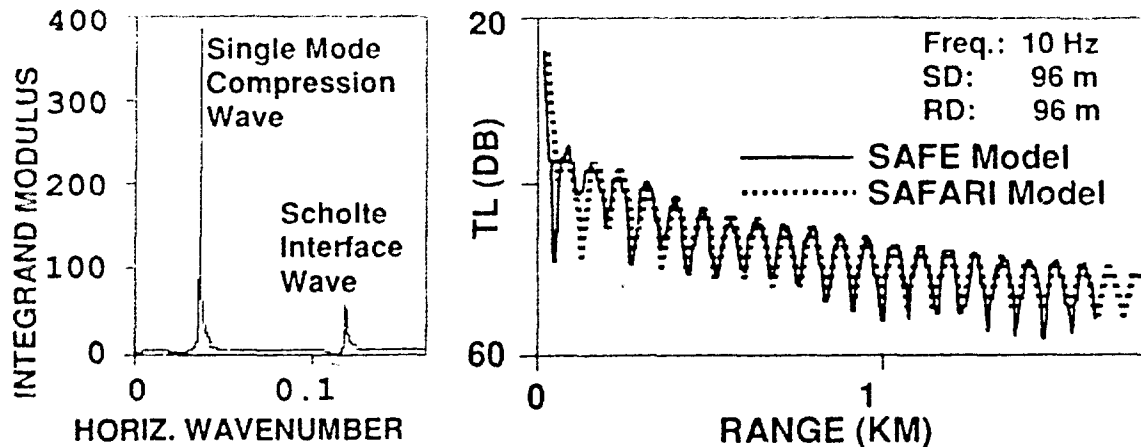


Fig. 4. SAFE and SAFARI models' TL compared for a flat shear bottom. The deep source excites a Scholte wave (seen in wavenumber plot) causing interference at the 96 m receiver.

In Figs. 4 and 5, the source was at a depth of 96 m (4 m above the water-solid interface) to excite the interface wave. For the deep receiver (96 m) the interference pattern between the one propagating mode and the interface wave is quite noticeable in the transmission loss (TL) predictions (Fig. 4) from both the SAFE model and the SAFARI model (Schmidt and Jensen, 1985). A wavenumber spectrum plot confirmed that only one trapped mode and one evanescent (Scholte) mode existed. In Fig. 5 the receiver was at the shallow depth (32 m) and too far from the bottom interface for the Scholte wave to interfere with the one propagating mode. Note the absence of the Scholte in the wavenumber spectrum plot. SAFE and SAFARI agree quite well for both receiver depths (Figs. 4 and 5).

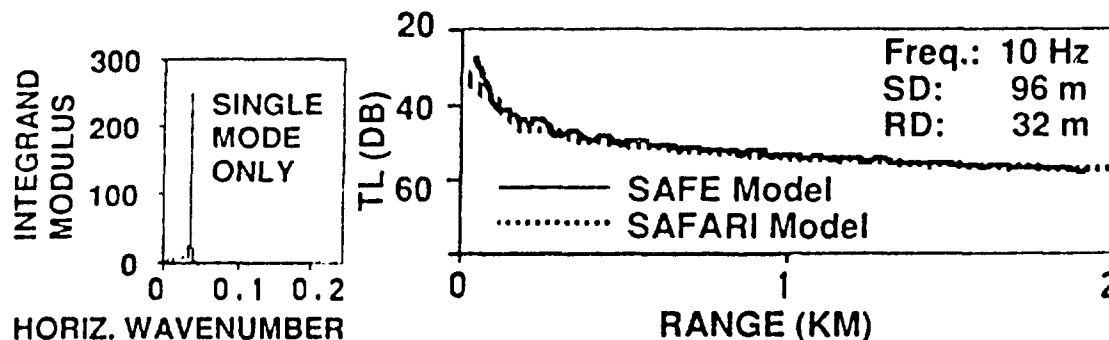


Fig. 5. SAFE and SAFARI models' TL predictions for a flat shear bottom - shallow receiver, deep source (4 m above bottom).

Figure 6 shows TL predictions made by the SAFE model for a step-periodic rough bottom with shear (see Fig. 3). The same two receiver depths (32 m and 96 m) were used as in the flat bottom with shear case and the SAFE TL predictions for the flat bottom with shear case (Figs. 4 and 5) are replotted in Fig. 6 for comparison. The effects of both the Scholte wave and the step-periodic roughness is evident in the TL from the deep receiver. The Scholte wave again causes a "periodic high-frequency" interference with the single propagating mode while the step-roughness destroys this periodic behavior. As previously noted, the shallow receiver is too far from the bottom interface to receive any effect from the Scholte wave. However, the step-roughness does create backscatter which interferes with the one propagating mode resulting in a "high-frequency" interference effect similar to that produced by the Scholte wave interference effect.

